Unified Undoubled QATNU Shutter Benchmark

Autonomous scattering, quantum routing, convergence, and native edge-ladder controls

Joshua Farrow
Numerical experiment report

June 2026

Abstract

We complete an end-to-end finite benchmark in which a single undoubled chain of square-root edge ladders, a finite central barrier, an autonomous controller, and an incident one-quantum packet coexist in one time-independent joint Hamiltonian. In the canonical $N = 18$ run, a permanently closed barrier transmits 0.00741, a permanently open chain transmits 0.97394, and the autonomous shutter transmits 0.71432. The packet backreacts on the controller and generates 0.67138 nats of controller–field entanglement, while the vacuum generates only 8.27×10^{-4} nats. Conditioning on the final controller sector resolves reflected and transmitted branches with right-side fractions 0.19789 and 0.83531. Tracing half of the actual undoubled chain gives strictly positive probabilities in every resolved number sector $n = 0, \ldots, 5$. Chain-length, occupation-cutoff, unrestricted local-product-basis, speed, barrier, arrival-time, reciprocity, energy, and ladder-operator controls are reported. The construction establishes a controlled low-occupation edge-register realization of an autonomous quantum shutter; it does not derive electromagnetism or complete the native matter/frustration embedding.

1 Unified model

Each site carries a truncated square-root ladder,

$$R_j = \sum_{n=0}^{d-2} \sqrt{n+1}\, |n+1\rangle\langle n|\,, \qquad q_j = \frac{R_j + R_j^\dagger}{\sqrt{2\omega_0}}. \tag{1}$$

The open chain is

$$H_O = \sum_{j=0}^{N-1} \omega_0 \left(n_j + \frac{1}{2}\right) + \frac{\kappa}{2}(q_0^2 + q_{N-1}^2) + \frac{\kappa}{2} \sum_{j=0}^{N-2} (q_{j+1} - q_j)^2. \tag{2}$$

For the central sites $\ell = N/2 - 1$ and $r = N/2$, a finite closed barrier is selected by

$$H_C = H_O + \eta\kappa q_\ell q_r. \tag{3}$$

At $\eta = 1$ the central cross term is exactly cancelled, leaving two local pins; the canonical run uses $\eta = 0.95$.

The controller is a finite tight-binding register,

$$H_{\mathrm{ctrl}} = -J \sum_{s=0}^{R-2} \left(|s+1\rangle\langle s| + |s\rangle\langle s+1|\right), \qquad P_C = \sum_{s<r_*} |s\rangle\langle s|\,, \tag{4}$$

and the complete Hamiltonian is

$$\boxed{H_{\mathrm{joint}} = I_C \otimes H_O + P_C \otimes \eta\kappa q_\ell q_r + H_{\mathrm{ctrl}} \otimes I_F.} \tag{5}$$

Every trajectory at fixed parameters is therefore generated by one fixed, time-independent Hamiltonian. The numerical field basis contains every occupation configuration with $\sum_j n_j \le n_{\max}$.

The canonical parameters are

$$N = 18, \quad n_{\max} = 5, \quad \omega_0 = 3, \quad \kappa = 1.2, \quad \eta = 0.95, \quad R = 10, \quad J = 0.14, \quad r_* = 3, \quad T = 24. \tag{6}$$

The field dimension is 33,649 and the joint dimension is 336,490.

2 Autonomous opening and scattering

The controller begins with $\langle P_C \rangle = 0.99999434$. Figure 1 shows its subsequent motion. The packet changes the final controller probability from 0.14348507 for the vacuum input to 0.21636027, a direct backaction signal.

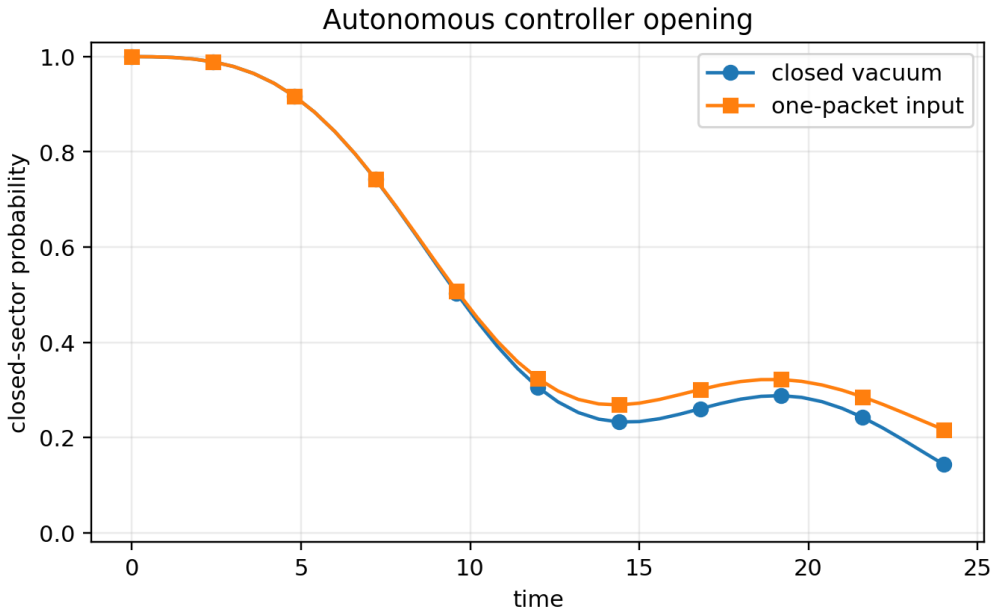

Figure 1: Closed-sector probability under the same canonical joint Hamiltonian. The packet and vacuum histories diverge after the collision.

Static controls establish that the bilinear functions as a shutter. The permanently closed, autonomous, and permanently open transmissions are

$$\mathcal{T}_C = 0.00741459, \qquad \mathcal{T}_A = 0.71431664, \qquad \mathcal{T}_O = 0.97393911. \tag{7}$$

The autonomous packet-minus-vacuum decomposition is

$$N_L = 0.27426157, \qquad N_R = 0.68575783, \qquad N_{\text{center}} = 0.04775421, \tag{8}$$

with reflection 0.28568336. The open-mode number difference is 1.00001283.

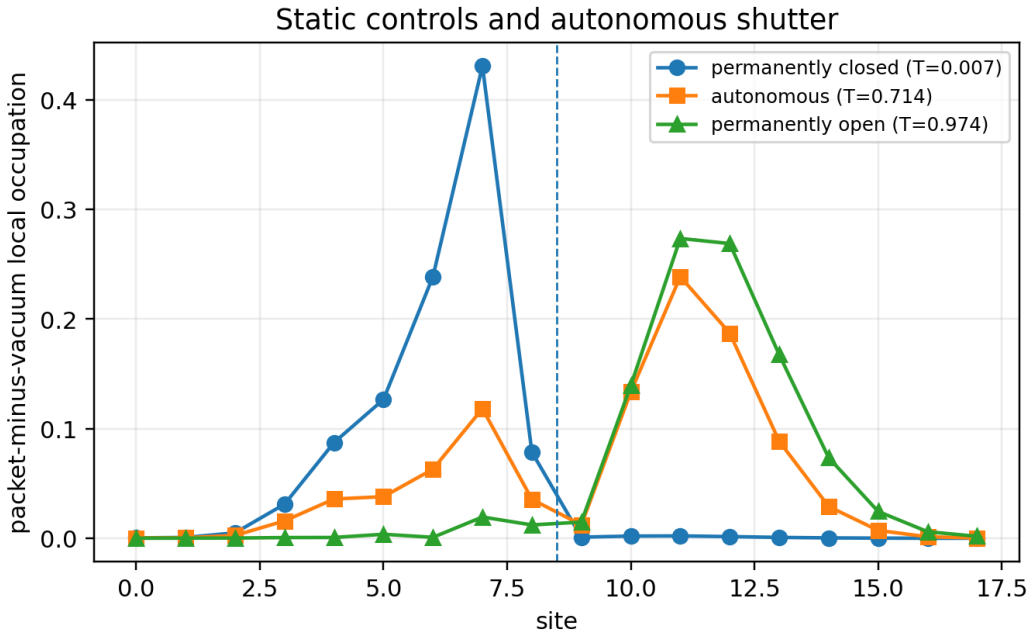

Figure 2: Final packet-minus-vacuum local occupations. The autonomous result lies between the permanently closed and open controls.

3 Quantum routing and controller backaction

The packet makes the geometry register a which-path degree of freedom. Its final controller–field entropy is

$$S_{C:F}^{\text{packet}} = 0.671381 \text{ nats}, \tag{9}$$

close to $\ln 2$, whereas the vacuum value is only 8.27×10^{-4} nats.

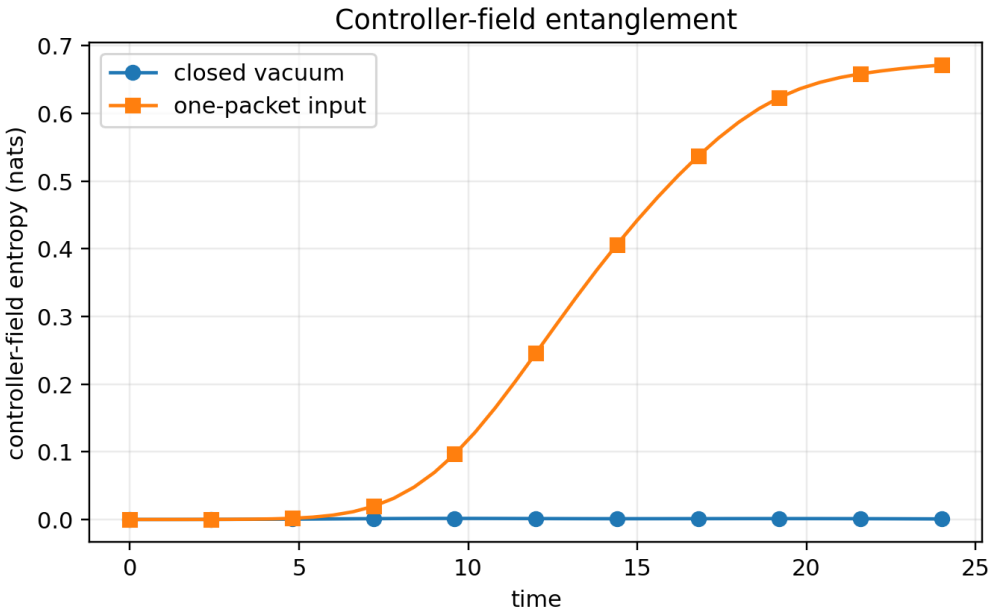

Figure 3: Controller–field entanglement. A one-packet input produces an almost binary geometry/path record, while the vacuum remains nearly separable.

Conditioning the same final state on the controller gives

sector	probability	right-side fraction	fidelity to static output
closed	0.21636027	0.19789456	0.80224026
open	0.78363973	0.83530595	0.84264850

The approximate binary controller/path mutual information is 0.223392 bits. The less-than-unit static fidelities are physically expected: the final sector label does not encode the controller's complete time history.

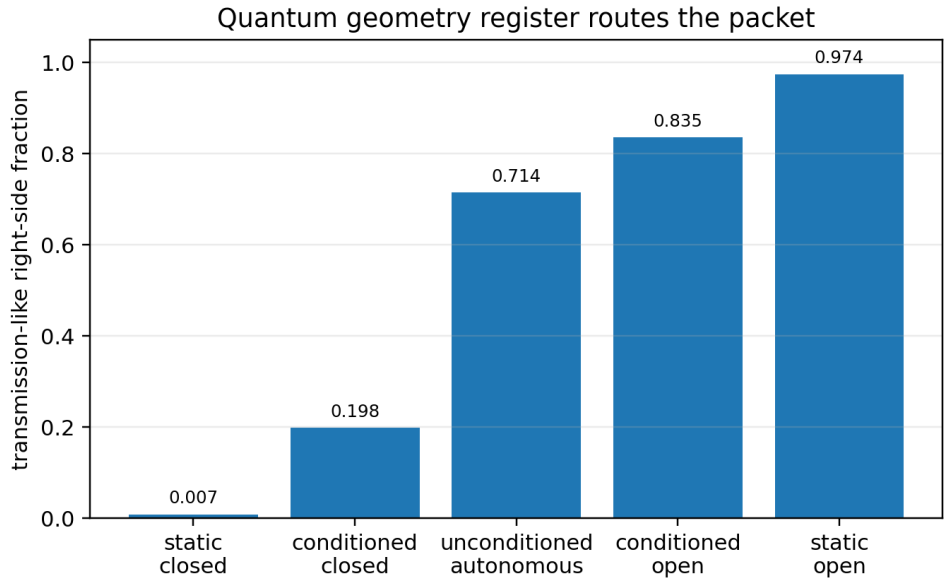

Figure 4: Static controls, unconditioned autonomous output, and controller-conditioned branches. The controller acts as a quantum routing register.

A separate coherent-control test initializes an equal superposition of permanently closed and open geometries. The vacuum branch overlap is 0.99936450 and its controller entropy is 0.002877 nats. The packet branch overlap is 0.12719163 and its entropy is 0.685036 nats. Thus the packet, rather than the bare vacuum, makes the two geometries operationally distinguishable.

4 Reduced particle-number support

Tracing either half of the actual undoubled chain produces a nontrivial reduced number distribution. On the transmitted half,

n	$P_R(n)$
0	0.301101446
1	0.676119232
2	0.006507993
3	0.015948121
4	0.000090307
5	0.000232902

Every resolved sector is positive and $P_R(n \geq 2) = 0.02277932$. This is an actual output of the autonomous undoubled shutter, not the earlier illustrative squeezed-pair normal form. It is, however, a finite-cutoff precursor rather than a proof of an infinite tail.

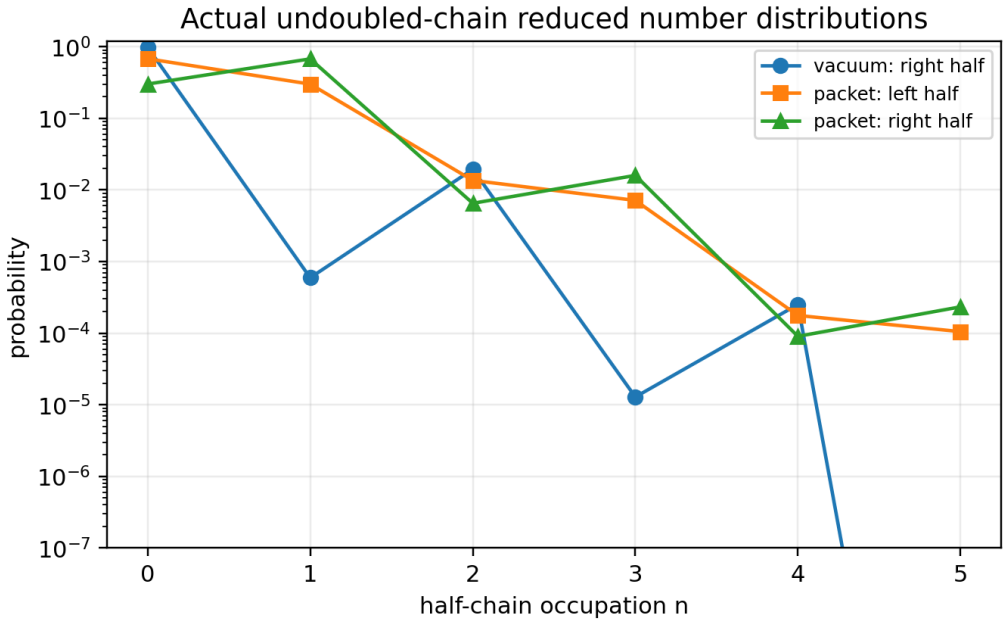

Figure 5: Half-chain occupation distributions. The packet output has support in every retained sector $n = 0, \ldots, 5$.

The packet-minus-vacuum one-body density matrix has leading natural occupations

$$0.7286811, \quad 0.2547846, \quad 0.0173851, \ldots \tag{10}$$

The leading orbital is 92.25% supported on the transmitted half; the first two occupations carry 97.59% of the excess one-body weight.

5 Locality and energy closure

The central two-site block has packet-versus-vacuum trace distance 0.0470957. The far-left and far-right edge blocks have distances 0.0006931 and 0.0016250. The information carried by the packet is therefore localized around the active packet/transition region in this finite chain.

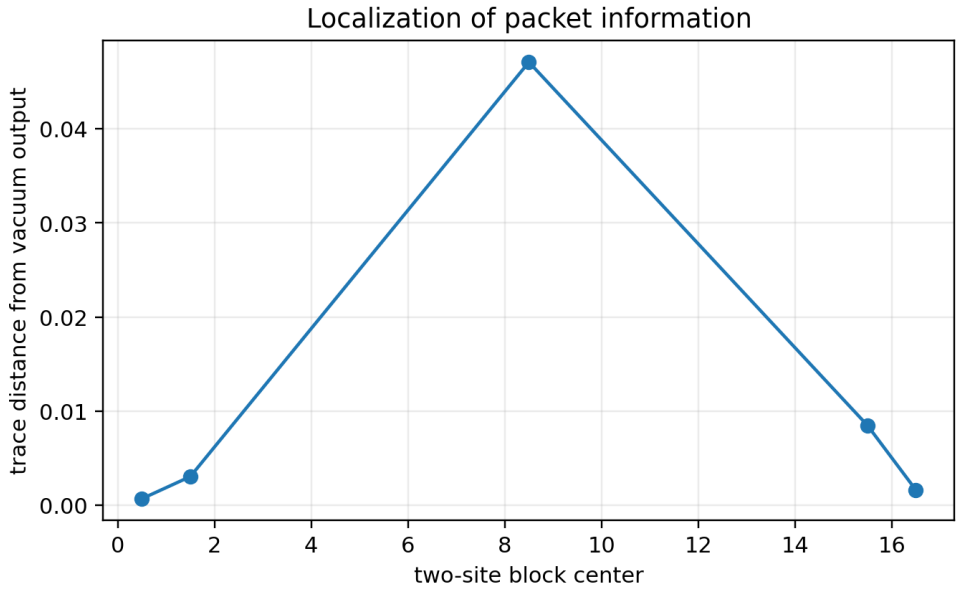

Figure 6: Trace distance between packet and vacuum outputs for selected two-site reductions.

For the packet input, the final changes are

$$\Delta E_F = -3.24666 \times 10^{-3}, \quad \Delta E_C = +3.66779 \times 10^{-3}, \quad \Delta E_{\text{int}} = -4.21131 \times 10^{-4}, \tag{11}$$

which close to 1.56×10^{-13}. The maximum absolute total-energy drift is 3.98×10^{-13}. The sign in this finite-barrier scattering run corresponds to field/interaction energy transferred into the controller; the robust statement is autonomous energy exchange and exact total closure.

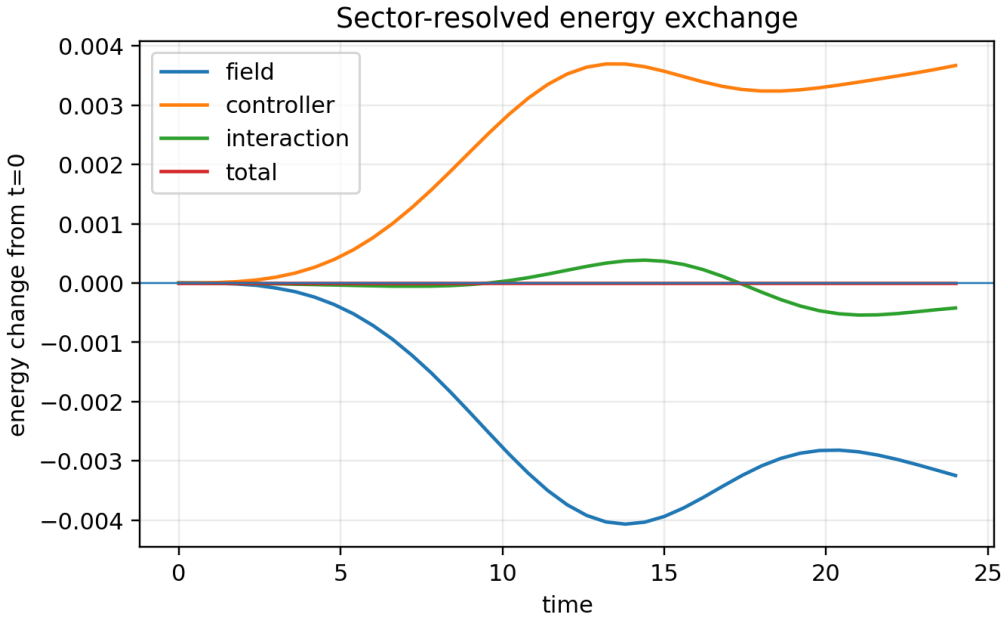

Figure 7: Sector-resolved energy changes for the packet input. The total remains constant to numerical precision.

6 Convergence and independent validation

At fixed lattice spacing, transmission converges with chain length:

N	transmission
12	0.70105331
14	0.71082752
16	0.71394040
18	0.71431664

The $N = 16$ to 18 change is 3.76×10^{-4}, or 0.0527%.

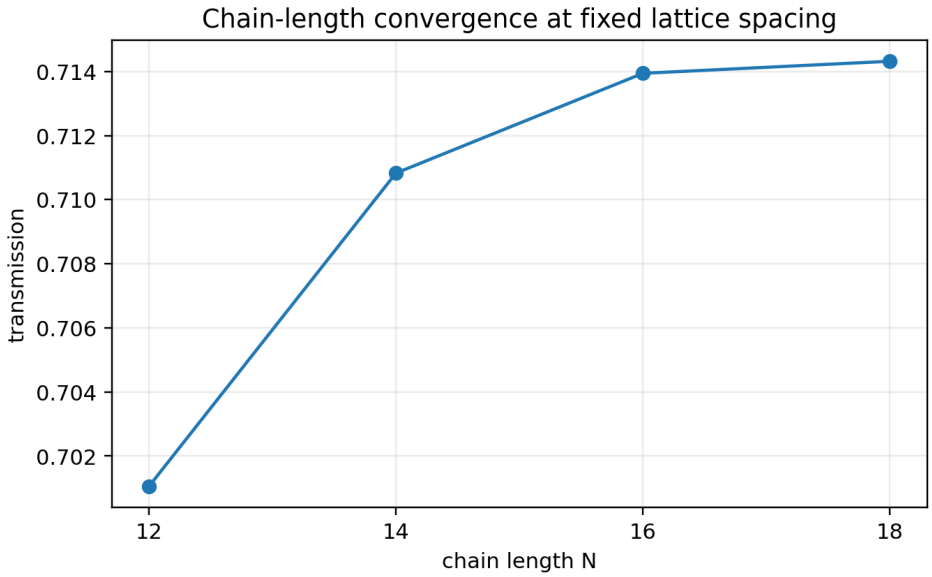

Figure 8: Finite-length convergence. This scan holds the lattice spacing fixed and is not a continuum limit.

At $N = 14$, increasing the global total-occupation ceiling gives

$n_{\max}$	transmission	final packet P_C
3	0.70926606	0.21811006
4	0.71028870	0.21811643
5	0.71082752	0.21658317
6	0.71087702	0.21658330

The $n_{\max} = 5$ to 6 transmission shift is 4.95×10^{-5}. The vacuum Bogoliubov number displays an even/odd cutoff effect because the squeezed vacuum occupies even total-number sectors; at $n_{\max} = 6$ its relative error is 1.15×10^{-6}.

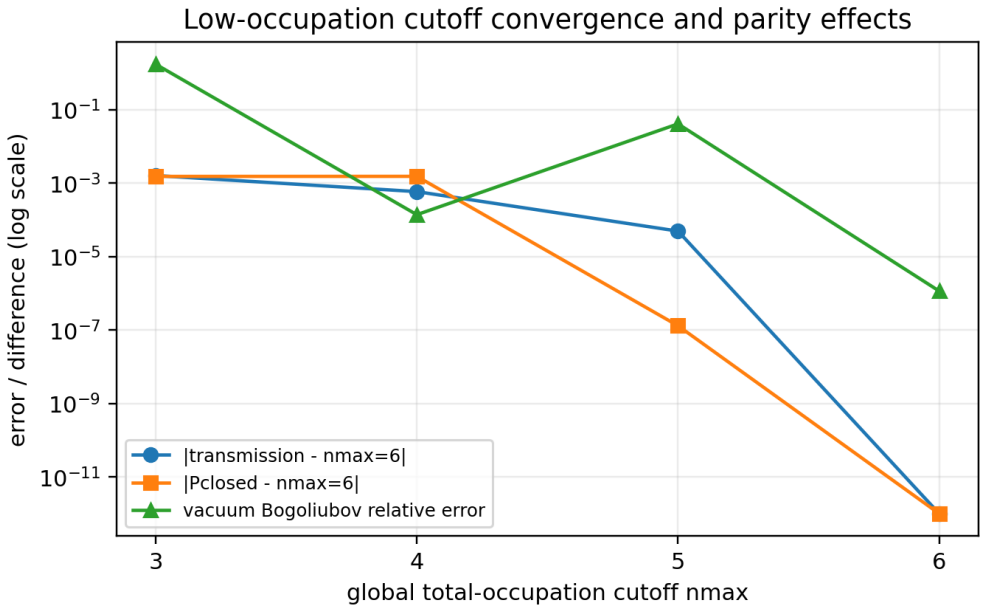

Figure 9: Cutoff convergence. Scattering observables converge smoothly; the vacuum diagnostic shows the expected parity sensitivity of a pair-populated squeezed state.

The global low-occupation projection was independently checked against an unrestricted tensor product of six local dimension-five ladders. The projected and full-product transmissions are 0.49614188 and 0.49983819; their difference is 0.740%. The open-mode one-particle excess differs by 0.0783%, and the full-product packet has only 1.81×10^{-4} probability above total occupation four.

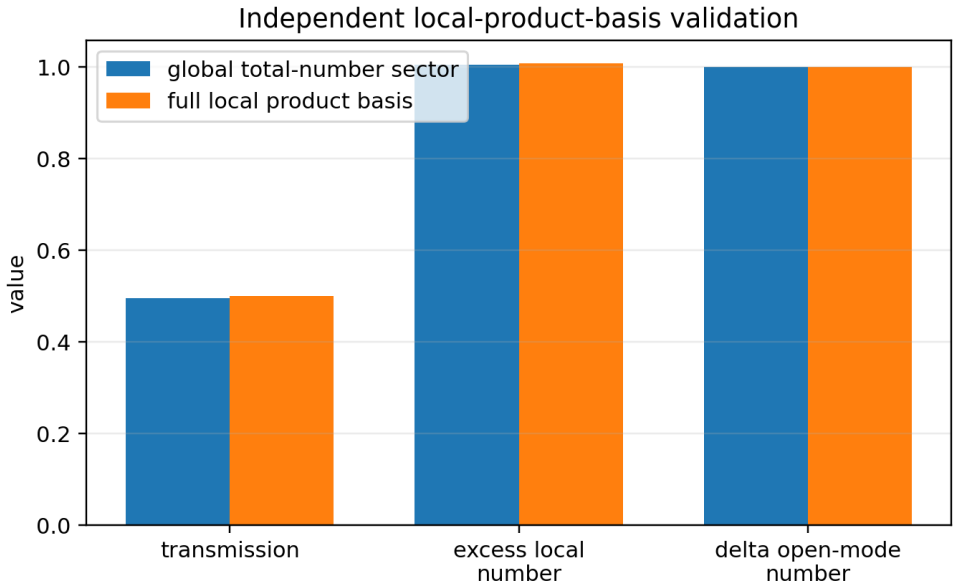

Figure 10: Independent local-product-basis check of the globally projected low-occupation calculation.

Finally, replacing the square-root ladder by a unit-amplitude shift produces a vacuum Bogoliubov-number relative error of 5.27, compared with 0.0177 for the square-root ladder in the same small benchmark. Coarse transmission is not a sufficient validation of the oscillator algebra.

7 Speed, barrier, timing, and reciprocity controls

Increasing controller hopping from $J = 0.06$ to 0.24 raises transmission from 0.219983 to 0.865028 while reducing final packet P_C from 0.600980 to 0.072609. This is a family of time-independent Hamiltonians indexed by J.

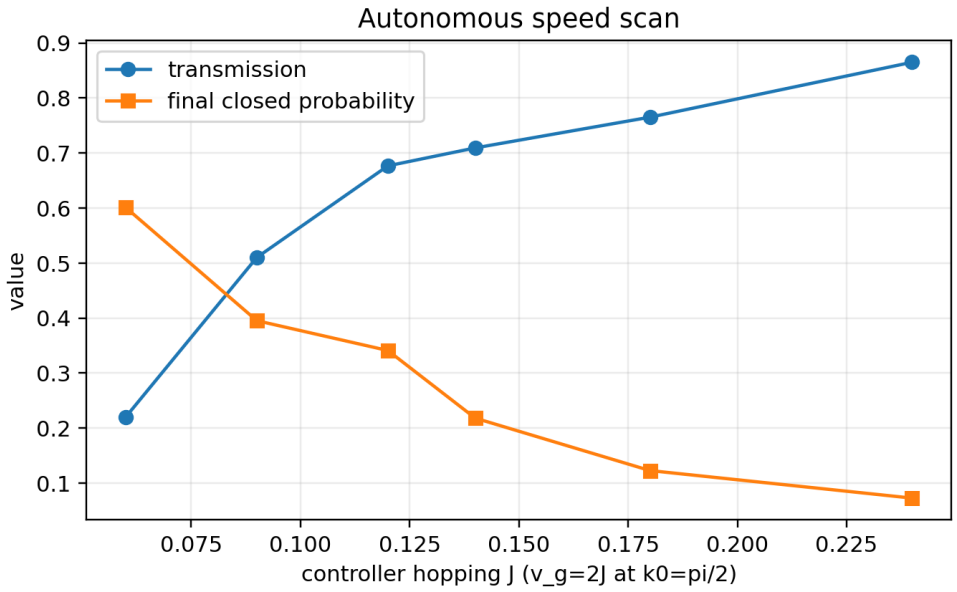

Figure 11: Controller-speed scan. Faster escape from the closed sector produces greater packet transmission.

Increasing the central cancellation fraction from $\eta = 0.5$ to 1 decreases transmission from 0.857392 to 0.706873, confirming that the gated bilinear controls the expected barrier strength.

The collision-time test holds the controller fixed and moves the initial packet center. Larger center means earlier arrival at the shutter. Transmission falls from 0.701153 at center 1.0 to 0.333087 at center 4.75, because the earlier packet encounters a less-open shutter.

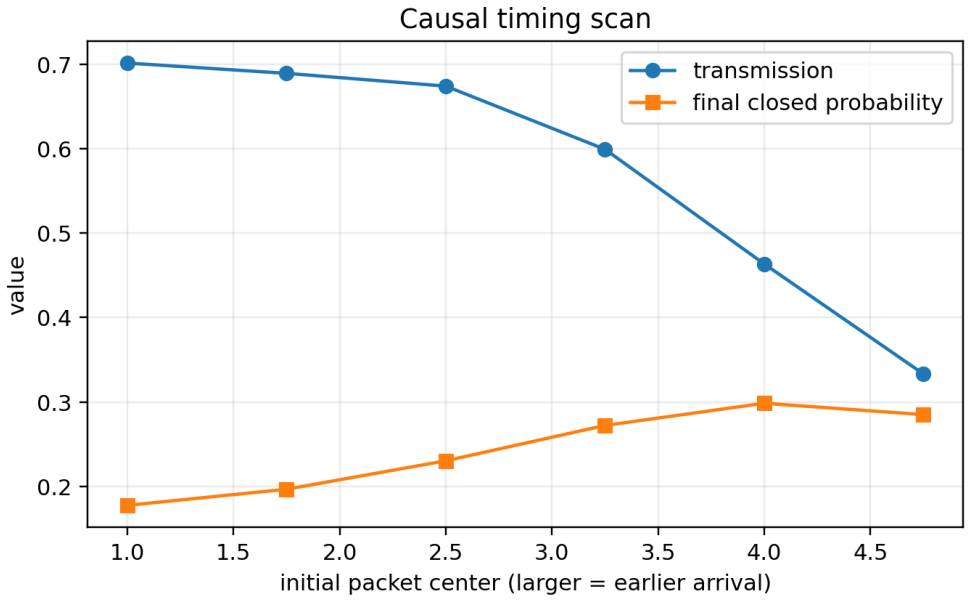

Figure 12: Arrival-time control. The packet is increasingly reflected when it reaches the central link earlier in the autonomous opening history.

A mirror-paired test gives

$$\mathcal{T}_{L\to R} = 0.7092802162234706, \qquad \mathcal{T}_{R\to L} = 0.7092802162234790, \tag{12}$$

with absolute difference 8.44×10^{-15}. The implementation therefore preserves left–right reciprocity to floating-point precision.

8 Status and next steps

The combined experiment establishes the following finite statement:

> A QATNU-style square-root edge-ladder chain with a direct inter-edge bilinear and an autonomous quantum controller realizes a reciprocal, energy-conserving, dynamically opening shutter. It scatters a one-quantum packet into controller-correlated reflected and transmitted branches and produces a reduced finite-cutoff number distribution with support in every resolved sector.

This closes the end-to-end low-occupation edge-register benchmark. It does not establish a native electromagnetic $U(1)$ sector, an unrestricted long-chain local Hilbert space, or the complete QATNU matter/frustration embedding. The next decisive integrations are:

1. replace the global total-number projection by larger unrestricted local edge registers;
2. drive the long-chain bilinear through the native matter/frustration network;
3. combine this chain with fixed-physical-length smooth continuum scaling;
4. construct asymptotic outgoing wave-packet algebras and complete local Weyl/correlator tests in the same native chain;
5. study multipacket linearity and controller-mediated effective interactions.

Reproducibility

The bundle contains the Hamiltonian implementation, canonical runner, static and coherent controls, deep reduced-state analysis, convergence scans, timing/reciprocity tests, unrestricted product-basis validator, raw JSON, final state vectors, and all figures. The canonical vacuum and packet evolutions required 31.4 and 27.9 seconds in the supplied environment.